THE SWIFT X-RAY FLARING AFTERGLOW OF GRB 050607

CLAUDIO PAGANI,[1,2] DAVID C. MORRIS,[2] SHIHO KOBAYASHI,[3] TAKANORI SAKAMOTO,[4] ABRAHAM D. FALCONE,[2] ALBERTO MORETTI,[1]
KIM PAGE,[5] DAVID N. BURROWS,[2] DIRK GRUPE,[2] ALON RETTER,[2] JUDITH RACUSIN,[2] JAMIE A. KENNEA,[2] SERGIO CAMPANA,[1]
PATRIZIA ROMANO,[1] GIANPIERO TAGLIAFERRI,[1] JOANNE E. HILL,[4,6] LORELLA ANGELINI,[4] GIANCARLO CUSUMANO,[7]
MICHAEL R. GOAD,[5] SCOTT BARTHELMY,[3] GUIDO CHINCARINI,[1] ALAN WELLS,[8] PAOLO GIOMMI,[9]
JOHN A. NOUSEK,[2] AND NEIL GEHRELS[4]

ABSTRACT

The unique capability of the *Swift* satellite to perform a prompt and autonomous slew to a newly detected gamma-ray burst (GRB) has yielded the discovery of interesting new properties of GRB X-ray afterglows, such as the steep early light-curve decay and the frequent presence of flares detected up to a few hours after the GRB trigger. We present observations of GRB 050607, the fourth case of a GRB discovered by *Swift* with flares superimposed on the overall fading X-ray afterglow. The flares of GRB 050607 were not symmetric as in previously reported cases, showing a very steep rise and a shallower decay, similar to the fast rise, exponential decay that are frequently observed in the gamma-ray prompt emission. The brighter flare had a flux increase by a factor of ∼25, peaking for 30 s at a count rate of approximately 30 counts s^{-1}, and it presented hints of additional short-timescale activity during the decay phase. There is evidence of spectral evolution during the flares. In particular, at the onset of the flares the observed emission was harder, with a gradual softening as each flare decayed. The very short timescale and the spectral variability during the flaring activity are indicators of possible extended periods of energy emission by the GRB central engine. The flares were followed by a phase of shallow decay, during which the forward shock was being refreshed by a long-lived central engine or by shells of lower Lorentz factors, and by a steepening after approximately 12 ks to a decay slope considered typical of X-ray afterglows.

Subject headings: gamma rays: bursts — X-rays: individual (GRB 050607)

1. INTRODUCTION

The *Swift Explorer* (Gehrels et al. 2004), designed to discover and study GRBs, was launched on 2004 November 20. When the Burst Alert Telescope (BAT; Barthelmy et al. 2005) triggers on a newly discovered GRB, the *Swift* satellite performs an autonomous slew to the GRB position determined on board, allowing prompt follow-up observations with the two narrow-field instruments, the X-Ray Telescope (XRT; Burrows et al. 2005b) and the Ultraviolet/Optical Telescope (UVOT; Roming et al. 2005).

In the standard scenario the GRB emission is caused by shocks in a relativistic expanding fireball (Mészáros & Rees 1997). The internal shocks of the moving ejecta are responsible for the prompt gamma-ray emission, while external shocks caused by the interaction of the fireball with the surrounding medium produce the afterglow emission observed in the X-ray and lower energy bands.

Thanks to the rapid spacecraft response to the BAT triggers, the XRT has been able to observe and autonomously localize GRB afterglows at early times, unveiling new and unexpectedly complex behaviors of the X-ray light curves, which frequently show multiple breaks with segments of distinct decay slopes (Nousek et al. 2006) and flares superimposed on the fading afterglow.

In this paper, we report on the properties of the X-ray afterglow of GRB 050607, which was dominated, in its early phase, by emission from X-ray flares superimposed on the overall decay. This was the fourth case in which X-ray flares were detected in the afterglows of GRBs discovered by *Swift* (Romano et al. 2006; Godet et al. 2006; Falcone et al. 2006). X-ray flares have been previously observed in few cases by *BeppoSAX* (XRF 011030, GRB 011121, and GRB 011211) and were identified as the onset of the afterglow (Galli & Piro 2005; Piro et al. 2005). A more detailed study of the characteristics and the origin of X-ray flares is now possible thanks to the unique *Swift* capabilities, which have greatly increased the number of rapid observations of the early phase of the X-ray afterglows. Continued internal engine activity at late times was proposed to explain the very short timescale and spectral variations during the flares observed in XRF 050406 (the first flare detected by *Swift*; see Romano et al. 2006) and the very bright flare of GRB 050502b (Falcone et al. 2006), which peaked 740 s after the GRB prompt emission. The flares in the X-ray afterglow of GRB 050607 had asymmetric shapes, with a steeper rise than previously observed flares, and a shallower decay, similar to the FREDs (Fast Rise, Exponential Decay) that are frequently observed in the GRBs' prompt emission.

In this work, we describe the XRT data analysis of the GRB afterglow, focusing in particular on the temporal and spectral properties of the early phase of flaring activity of the X-ray emission. We use the notation $F(t, \nu) \propto (t - t_0)^{-\alpha} \nu^{-\beta}$ for the temporal and spectral dependence of the flux. All uncertainties are given at the 90% confidence level for one interesting parameter ($\Delta\chi^2 = 2.7$). The observations are presented in § 2 and the data analysis in

[1] INAF–Osservatorio Astronomico di Brera, Via Bianchi 46, 23807 Merate, Italy; pagani@astro.psu.edu.

[2] Department of Astronomy and Astrophysics, Pennsylvania State University, 525 Davey Laboratory, University Park, PA 16802.

[3] Astrophysics Research Institute, Liverpool John Moores University, Twelve Quays House, Birkenhead CH41 1LD, UK.

[4] NASA Goddard Space Flight Center, Greenbelt, MD 20771.

[5] Department of Physics and Astronomy, University of Leicester, Leicester LE1 7RH, UK.

[6] Universities Space Research Association, 10211 Wincopin Circle, Suite 500, Columbia, MD 21044-3432.

[7] INAF–Istituto di Astrofisica Spaziale e Fisica Cosmica Sezione di Palermo, Via U. La Malfa 153, 90146 Palermo, Italy.

[8] Space Research Centre, University of Leicester, Leicester LE1 7RH, UK.

[9] ASI Science Data Center, Via Galileo Galilei, 00044 Frascati, Italy.

TABLE 1
Observations of GRB 050607

Sequence Number	Number of Orbits	Start Time (UT)	Stop Time (UT)	Exposure Time (s)
0......................	3	2005-158-09:12:56	2005-158-13:04:40	7955
1......................	13	2005-158-17:13:52	2005-159-13:11:19	44423
2......................	11	2005-160-00:05:00	2005-160-16:30:51	30730
3......................	13	2005-161-00:05:00	2005-161-23:03:17	26397
4......................	8	2005-162-00:04:59	2005-162-21:03:57	4556
5......................	3	2005-165-19:38:15	2005-165-23:29:47	7721
6......................	14	2005-167-00:36:29	2005-167-23:42:54	31998
7......................	12	2005-168-02:17:51	2005-168-23:44:58	24316
8......................	29	2005-169-23:17:40	2005-171-23:59:57	39943
9......................	14	2005-172-01:22:51	2005-172-23:59:59	12775
10....................	39	2005-176-01:34:52	2005-178-21:41:30	62773
11....................	12	2005-181-01:01:56	2005-181-23:37:51	12189
12....................	3	2005-182-01:07:13	2005-182-12:29:26	4160
13....................	3	2005-182-17:15:46	2005-182-20:31:42	1682
14....................	11	2005-182-23:41:26	2005-183-23:51:23	7676
15....................	9	2005-184-01:23:59	2005-184-22:21:44	6979
16....................	21	2005-184-23:45:48	2005-186-12:55:57	21884
17....................	6	2005-186-14:25:03	2005-186-22:35:26	5005
18....................	11	2005-187-00:04:59	2005-187-22:42:18	10566

§ 3. The discussion and conclusion are in § 4. A detailed presentation of the procedure applied to correct for the "pile-up" effect, caused by the high X-ray afterglow count rate during the flares, is given in the Appendix.

2. OBSERVATIONS

The BAT triggered on the GRB 050607 at 09:11:22.81 UT on 2005 June 7 (Retter et al. 2005). The spacecraft started the slew to the GRB 16.5 s after the trigger, while the burst was still ongoing, and settled on the burst 84 s after the trigger.

The XRT follows an autonomous sequence of observations in response to a GRB trigger, starting with the acquisition of a short image to localize the GRB afterglow and then performing observations in different readout modes according to the source intensity (Hill et al. 2004). Due to engineering tests on the narrow-field instruments at the time of the trigger, the XRT onboard centroiding algorithm could not converge on a source when the first image was acquired, and the nominal observing sequence could not be effectively followed. The instrument collected a single frame in Windowed Timing (WT) mode and then immediately switched into Photon Counting (PC) mode, designed to provide two-dimensional spatial information at the expense of a lower timing resolution. The GRB afterglow was monitored by the XRT for 30 days after the burst for a total exposure time of 363 ks. The complete set of the GRB observations is reported in Table 1.

The UVOT was in an engineering mode at the time of the GRB event, and therefore immediate data were not available. The first UVOT observation of the GRB field started at 22:36:23 UT, 12 hr and 25 minutes after the BAT trigger. No optical counterpart was detected (Ivanushkina et al. 2005).

The GRB 050607 field was observed with ground-based telescopes in the optical and the infrared (IR) bands. A fading source was detected with the 4 m Mayall Telescope at Kitt Peak Observatory in the I band with an initial magnitude of 21.46 ± 0.3, 640 s after the burst trigger (Rhoads 2005a). The transient was observed to have faded by 2.3 ± 0.2 mag in the I band between 640 s and 93.2 ks (Rhoads 2005c). Observations were also performed in the B, R, z, and g bands. The afterglow was detected in

the R band, but not clearly visible in the B-band images (Rhoads 2005b), indicating a possible Lyman break in the spectrum.

The MDM 2.4 m telescope also reported a source detected in the R band ($22.5 \text{ mag} < R < 23 \text{ mag}$; Halpern et al. 2005a) with the observation beginning 16 minutes after the GRB trigger. The object appeared to have faded (upper limit of $R > 24$ mag) in a follow-up observation performed on 2005 June 8 at 08:15 UT, 23 hr after the trigger (Halpern et al. 2005b).

Observations were also performed in the IR by the Rapid Eye Mount robotic telescope (Testa et al. 2005); prompt observations (192 s after the trigger) did not reveal any new bright object in the H band to a limiting magnitude of 16.0.

3. DATA ANALYSIS

3.1. *Gamma-Ray Analysis*

The BAT data (analyzed with BAT HEAsoft software ver. 6.0.2) showed a three-peak light curve with a T_{90} of 26.5 s, close to the mean value for long bursts of the BATSE catalog (Paciesas et al. 1999). The measured BAT flux had a peak of 1.15 ± 0.16 photon cm^{-2} s^{-1} and a total fluence (preslew and slew emission) of $5.8 \pm 0.5 \times 10^{-7}$ ergs cm^{-2} in the 15–150 keV band.

The BAT spectrum of GRB 050607 is well fitted with a single power-law model with index 1.83 ± 0.14. A fit of the spectrum with a Band function (Band et al. 1993)[10] does not provide a significant improvement in the $\chi^2_{\rm red}$ because of the difficulties in constraining $E_{\rm peak}$, due to the narrow BAT energy range and the relative low fluence of the GRB 050607 prompt emission.

The extrapolation of the BAT light curve into the XRT energy band is performed using the best-fit parameters obtained from the prompt emission spectral fit. If one assumes the GRB prompt emission to have a "universal" spectral shape (Preece et al. 2000) described by a Band function with $\alpha = 1.0$ and $\beta = 2.5$, the photon index of 1.83 of the simple power-law model fit of the BAT spectrum is very steep and would yield too high a value of the flux in the XRT energy band. The prompt flux in the XRT band

[10] The expression $f(E) = K_{30}(E/30)^{\alpha} \exp[-E(2 + \alpha)/E_{\rm peak}]$, if $E < (\alpha - \beta)E_{\rm peak}/(2 + \alpha)$; and $f(E) = K_{30}\{(\alpha - \beta)E_{\rm peak}/[30(2 + \alpha)]\}^{\alpha-\beta} \exp(\beta - \alpha) \times (E/30)^{\beta}$, if $E \geq (\alpha - \beta)E_{\rm peak}/(2 + \alpha)$.

TABLE 2
GRB 050607: BAT Extrapolated Fluxes

Time Range (s)	Power-Law Flux (10^{-10} ergs cm^{-2} s^{-1})	$\chi^2_{\rm red}$	Band Function Flux (10^{-10} ergs cm^{-2} s^{-1})	$\chi^2_{\rm red}$
−3.0–10.0.......	$128.75^{+94.96}_{-52.68}$	0.89	$41.95^{+11.27}_{-8.70}$	0.93
10.0–16.5........	$260.58^{+41.85}_{-15.16}$	1.21	$51.89^{+34.50}_{-16.19}$	1.27
16.5–30.0........	$470.14^{+154.64}_{-328.53}$	0.73	$52.80^{+75.91}_{-22.30}$	0.72
30.0–100.0......	<230	...	<0.54	...

NOTES.—GRB 050607: Extrapolation into the 0.2–10.0 keV band of the BAT data from the prompt emission. Two spectral models were assumed: a power law and a Band function. The $\chi^2_{\rm red}$ of the spectral model best fit is reported. For the fourth time interval, where no source is detected in the BAT data, an upper limit was derived for each of the two spectral models.

can therefore be assumed to lie between the fluxes extrapolated from the two spectral models: a simple power-law model and a Band function with fixed $\alpha = 1.0$ and $\beta = 2.5$.

The BAT spectrum was analyzed separately over different time intervals relative to the three peaks of the light-curve prompt emission. In the time interval $T_0 + 30$–$T_0 + 100$ s there is no source detection in the BAT observation, and a 3 σ upper limit was calculated using the two spectral models. The BAT extrapolated fluxes are reported in Table 2.

3.2. *GRB Position*

The X-ray afterglow position, determined from ground-processed data, is R.A. = $20^{\rm h}00^{\rm m}42^{\rm s}.7$, decl. = $+09°08'31''.4$ (J2000.0), with an uncertainty of $3''.8$. The position obtained with the xrtcentroid task was corrected for the systematic offsets observed in XRT and optical counterparts, caused by the slight misalignment between the XRT optical axis and the spacecraft star tracker boresight (Moretti et al. 2006). The X-ray afterglow is $44''$ from the reported BAT position (Retter et al. 2005) and $0''.9$ from the optical counterpart reported by Rhoads (2005a). The image of the afterglow detected by the XRT during the first orbit is presented in Figure 1, along with the BAT refined position (Retter et al. 2005), the XRT error circle, and the optical counterpart position (Rhoads 2005a).

3.3. *Timing Analysis*

The X-ray afterglow of GRB 050607 had a complex behavior, dominated by flares in the early observations, followed by a phase of slow decay that lasted approximately 12 ks and a late steepening to values typical of GRB afterglows. The X-ray light curve has been extracted in the energy range 0.2–10.0 keV and binned to obtain 20 background-subtracted counts per bin. Count rate to flux conversion factors were obtained from the best spectral model fit for the different afterglow phases (the detailed spectral analysis is discussed in § 3.4). The X-ray light curve of GRB 050607 and the extrapolated BAT fluxes in the 0.2–10.0 keV band are shown in Figure 2.

Due to the high count rate during the flares, the early XRT observations were severely affected by pile-up, the result of two or more photons being collected in a single CCD cell in a readout frame. In the Appendix we describe how the observations are altered by the pile-up effect, and we determine the affected region and the coefficient applied to the observed fluxes to correct for the pile-up.

The phase of flaring activity of the GRB 050607 X-ray afterglow is shown in Figure 3. To avoid the region contaminated by pile-up, the light curve of the first 510 s of observations after the GRB trigger was extracted from an annulus that excluded events
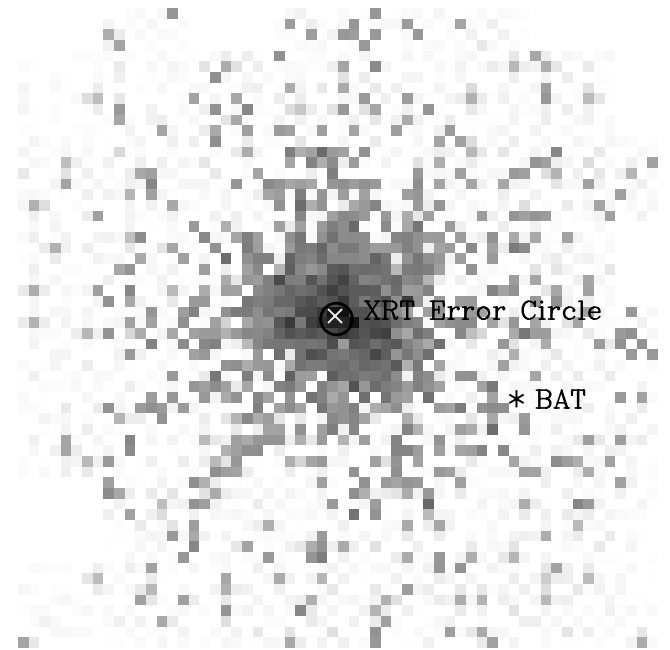

FIG. 1.—GRB 050607 afterglow XRT image extracted from the first orbit of photon counting observation. The BAT refined ground position, the XRT $3''.8$ error circle, and the optical afterglow position (*white cross inside the XRT error circle*) determined with the Mayall Telescope at Kitt Peak (Rhoads 2005a) are shown.

in the central 8 pixels ($18''.88$) and with an outer radius of 40 pixels. The first flare (referred to as flare A) was observed from 96 to 255 s after the GRB trigger, peaking at 4.6×10^{-10} ergs cm^{-2} s^{-1} (8.1 counts s^{-1}) approximately 135 s after the trigger. The second flare (flare B) was the brightest, lasting from 255 s to approximately 510 s after the trigger and including the majority of the X-ray emission, with a peak flux of 2.0×10^{-9} ergs cm^{-2} s^{-1} (35.6 counts s^{-1}) ~310 s after the trigger and a total fluence of 1.36×10^{-7} ergs cm^{-2} ($\simeq$23% of the BAT prompt emission).

The flares were asymmetric, similar to the FREDs that are often observed in the prompt GRB emission, with a rising side steeper than the following decay. In the case of flare A, the peak was
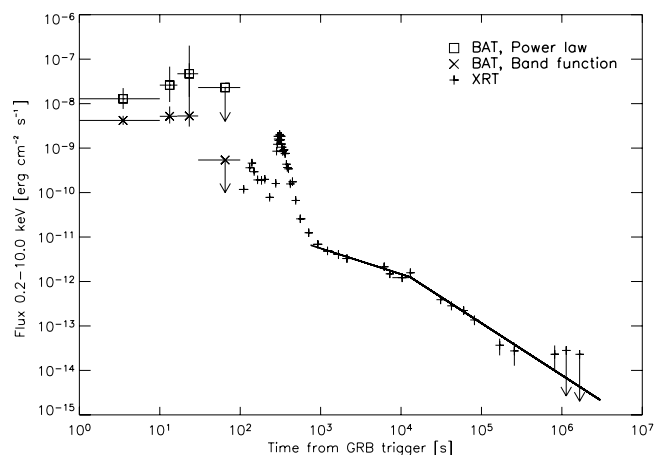

FIG. 2.—Combined BAT and XRT GRB 050607 light curve. The BAT fluxes were extrapolated to the 0.2–10.0 keV energy band assuming a simple power law (*squares*) and a Band (*asterisks*) spectral model. In the last BAT time bin (30–100 s) there was no detection in the BAT data, and upper limits were derived. The X-ray afterglow from the entire set of observations is in the energy band 0.2–10 keV, pile-up corrected. The time bars correspond to the time bin sizes. The best-fit broken power-law model is shown.
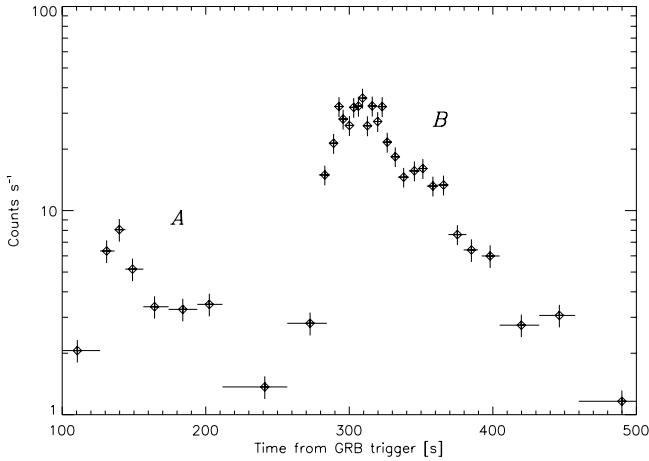
Fig. 3.—XRT light curve of the early GRB 050607 afterglow, in the energy band 0.2–10 keV, corrected for pile-up, with 20 photons per bin. The early X-ray emission was characterized by the presence of flares. Flare A had a peak at ∼8 counts s^{-1}; the brighter flare B lasted from 255 to 510 s after the first trigger with emission around 30 counts s^{-1} for approximately 30 s. Both flares are asymmetric: the decay is shallower than the very steep rise. This may be due to additional short-timescale activity superimposed on the main flare, such as the small "bump" observed at approximately 355 s after the burst trigger.

reached in ∼30 s, with the decay taking approximately 130 s, and for flare B the rising phase lasted for ∼35 s, followed by a "plateau" at the flare maximum with the X-ray emission at a count rate of ∼30 counts s^{-1} for approximately 30 s, and a decaying phase ∼190 s long that presents marginal indications of spikes and "bumps."

The flare's rise and decay can be fitted with a simple power law. With the notation $(t - t_0)^\alpha$, fixing t_0 at the onset of the flares, the flare A slope indices are $\alpha_{A, rise} = 1.2 \pm 0.2$ and $\alpha_{A, decay} = -1.3 \pm 0.3$, and for flare B are $\alpha_{B, rise} = 4.1 \pm 0.8$ and $\alpha_{B, decay} = -2.3 \pm 0.3$. The choice of t_0 is critical in determining the slopes indices. In fact, if t_0 is fixed at the GRB trigger time t_B the slopes are steeper, yielding higher values than for previously detected flares (Romano et al. 2006; Falcone et al. 2006). In this latter case flare A rises as $(t - t_B)^{5.9 \pm 0.6}$ and decays as $(t - t_B)^{-2.8 \pm 0.6}$, while for flare B the rise and decay are fitted with $(t - t_B)^{22 \pm 5}$ and $(t - t_B)^{-7.2 \pm 0.5}$.

The brighter flare B decay was fitted excluding the data points of the secondary bump superimposed on the flare and centered 355 s after the burst trigger. From the power-law fit decay parameters, the expected number of events in that time period is 323 ± 18, while the observed number of events is 398 ± 20. The observed 75 excess photons are significant at a 2.8 σ level. Although hints of short-timescale structure in the XRT light curve are present, in particular during the brightest flare, no significant periodicity was found from the timing analysis in the 2–300 s period range, using a frequency spacing of 10^{-3} s^{-1}.

After the flares, the X-ray afterglow emission decayed to intensities for which the effect of pile-up was negligible. Data were extracted using a circle of 20 pixel radius (smaller than the one used for the flares to avoid excessive background contamination) centered on the GRB afterglow, and the background was evaluated using a circle with $r = 40$ pixels in an area of the CCD without the presence of other sources. In the second, third, and fourth observations (segments 1, 2, and 3, respectively; see Table 1) a binning of 25 events per bin was used. At later times multiple observations (segments) were co-added to detect the X-ray afterglow, and a circle of 4 pixel radius centered on the GRB position was used to obtain a higher signal-to-noise ratio. The measured

afterglow flux was point-spread function (PSF)–corrected to account for the smaller extraction region. The last two data points of the light curve are 90% upper limits (Fig. 2).

After the main flare, starting from 510 s after the GRB trigger, the afterglow is best fitted with a broken power law (shown in Fig. 2) with indices of 0.58 ± 0.07 and 1.17 ± 0.07, with a break time of 11.7 ± 0.6 ks ($\chi^2_{red} = 1.02$). The broken power-law model is a significantly better fit (F-test probability of 4.8×10^{-3}) to the late X-ray afterglow than a single power law (index of 0.88 ± 0.03 with a χ^2_{red} of 1.91). The observed decay slopes and the degree of steepening after the break are close to the average values obtained from the sample of 27 GRBs discovered by *Swift* reported in Nousek et al. (2006).

3.4. *Spectral Analysis*

The X-ray afterglow of GRB 050607 can be divided into four time intervals: flare A extending to 255 s after the trigger, the stronger flare B from 255 s to approximately 510 s, the shallow section of the afterglow emission, and the late steepening after 12 ks. The spectral analysis (using XSPEC ver. 11.3.2) was performed separately on each light-curve phase, selecting events with grades 0–12. Because of low statistics below 0.5 keV and at high energies the spectra were fitted in the energy range 0.5–6.0 keV; the `swxpc0to12_20010101v007.rmf` response matrix file from the *Swift* XRT calibration database was used for the spectral fit. The ancillary file was created using the `xrtmkarf` command of the `xrtpipeline` software, applying the PSF correction. The spectra during the first 510 s of observation were extracted from an annular region as in the timing analysis to avoid pile-up contamination. The background was evaluated from a circle of $r = 40$ pixels in a region without sources.

Due to the low number of events during the first flare and the late part of the light curve, during these time intervals C-statistics (Cash 1979) were used in the fitting procedure, while χ^2-statistics were used for the main flare. Since the X-ray count rate at low energy was too low to properly constrain the X-ray absorption column, the N_H was fixed to 1.41×10^{21} cm^{-2}, the weighted average value in the GRB 050607 direction (Dickey & Lockman 1990). The flares were fitted with both a simple absorbed power law and a cutoff power-law model to investigate a possible common origin of the X-ray flares and the prompt gamma-ray emission: in the energy band of the XRT data a cutoff power law is almost equivalent to a Band function.

The best fit of flare A with an absorbed power-law model yielded a photon index of $2.00^{+0.19}_{-0.18}$, with the absorption fixed at the Galactic value. The brighter flare B fit with an absorbed power-law model yielded an absorption column density 2 σ higher than the Galactic value. To allow comparisons with earlier and later spectra, the absorption was fixed to the Galactic value, obtaining a photon index of $2.27^{+0.13}_{-0.12}$, while selecting only the decaying phase of the flare yielded a photon index of $2.31^{+0.21}_{-0.19}$.

The fit of flare B with a cutoff power-law model yielded a best-fit absorption column density closer to the Galactic value than in the single power-law case. Fixing the absorption to the Galactic value, the cutoff power-law model is a better fit than an absorbed power law (χ^2_{red} improved from 1.54 to 1.14). The parameters of the cutoff power-law model fit are not very well constrained, especially in the case of the cutoff energy, due to the limited number of photons in the data set at high energies. The cutoff power-law model fit yielded a photon index of $1.41^{+0.48}_{-0.53}$, harder than the simple power law, and a cutoff energy of $2.4^{+3.5}_{-0.9}$ keV. Our attempt to also fit the dimmer, first flare with a cutoff power law did not properly constrain the fit parameters due to the low number of photons during that time interval. However, we
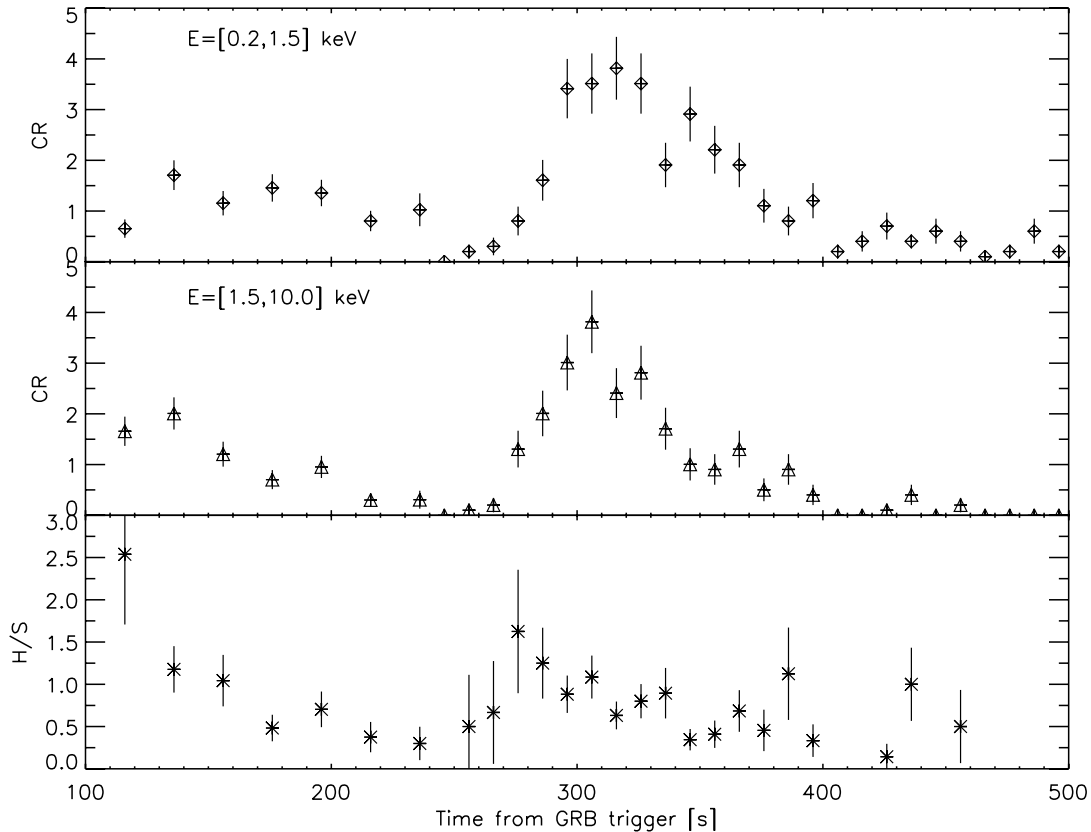
Fig. 4.—Band ratio of the early phase of the X-ray afterglow. The hard ($H = 1.5 - 10.0$ keV) and the soft ($S = 0.2 - 1.5$ keV) band energy ranges were chosen to obtain a similar number of counts in the two bands. The band ratio (H/S) shows evidence of spectral evolution during the two flares, with a harder emission at the flare's onset and a soft component that lasted longer and dominated the decay of the flare.

investigated the spectral evolution of the afterglow during the flares, dividing the light curve into a low-energy band and a high-energy band and evaluating the band ratio. The energy ranges (0.2–1.5 and 1.5–10.0 keV for the low- and high-energy bands, respectively) were selected to obtain a similar number of counts in
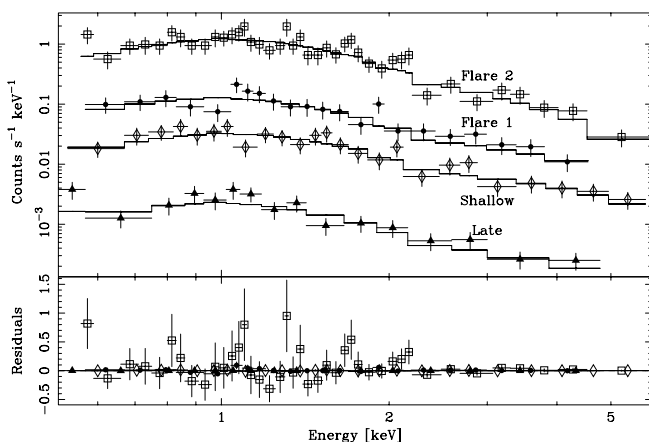

Fig. 5.—XRT spectra of the different afterglow phases. The data were fitted in the energy range 0.5–6.0 keV with a binning of 20 photons per bin for the bright second flare and a binning of 1 photon per bin for the other phases, for which *C*-statistics was used. The data are rebinned here to 10 photons per bin for presentation purposes, and the first flare spectrum is normalized by a constant factor of 0.2 for clarity. The absorbed cutoff power-law model was used to fit the spectrum of the bright flare, while a simple absorbed power-law model was used for the other afterglow phases. The cutoff power-law model yielded a harder spectrum ($\Gamma = 1.41$) for the bright flare than the late afterglow. In the bottom panel the differences between the data and the fitted models are displayed.

the two bands. Spectral evolution is evident in the band ratio plot (see Fig. 4). In particular, the hard band contributed to the overall emission mostly during the rising part of the two flares, while the soft emission lingered longer and started decaying at later times. The observed behavior indicates that the emission during the flares is harder than the underlying afterglow, and that the flares evolve spectrally, softening as they decay.

The late part of the X-ray afterglow was analyzed using events from a circular region of 20 pixel radius. We applied *C*-statistics to fit the data with an absorbed power law with absorption fixed to the Galactic value, yielding a photon index of $1.78^{+0.18}_{-0.13}$ for the shallow section of the light curve and a photon index of $1.97^{+0.36}_{-0.34}$ after the light-curve break. The spectra of the different afterglow phases are shown in Figure 5, and the fit results are presented in Table 3.

4. DISCUSSION AND CONCLUSIONS

The X-ray light curve of GRB 050607 has a complex behavior, presenting most of the unexpected features that have been observed in the afterglows of GRBs discovered by *Swift*, such as the presence of multiple breaks in the light curve and the flaring activity superimposed on the overall light-curve decay.

XRT observations indicate that flares are common in the early phase of X-ray afterglows (Burrows et al. 2005a; Zhang et al. 2006; Nousek et al. 2006): as of 2005 October 20, flares were detected by the XRT in 23 of the 50 afterglows for which observation with the narrow-field instruments started within 10 minutes from the BAT trigger. Several scenarios have been proposed as the possible source of flux variabilities of the X-ray afterglows: density fluctuations in the environment (Lazzati et al. 2002), angular

TABLE 3
GRB 050607: X-Ray Afterglow: Spectral and Timing Parameters

Phase	Time from Trigger	Γ Power Law	χ^2_{red}	Γ Cutoff Power Law	χ^2_{red}	β Power Law	α (Decay Slope)
First flare	96 s < T < 255 s	$2.00^{+0.19}_{-0.18}$	142.2[a]	...	...	...	...
Second flare	255 s < T < 510 s	$2.27^{+0.13}_{-0.12}$	1.54	$1.41^{+0.48}_{-0.53}$	1.14	...	...
Second flare decay	315 s < T < 510 s	$2.31^{+0.21}_{-0.19}$	0.89	...	...	$1.31^{+0.21}_{-0.19}$	7.20 (2.26 if $T_0 = T_{flare}$)
Flat	510 s < T < 12 ks	$1.78^{+0.18}_{-0.13}$	150.5[a]	...	...	$0.78^{+0.18}_{-0.13}$	$0.58^{+0.07}_{-0.07}$
Break	T > 12 ks	$1.97^{+0.36}_{-0.34}$	127.8[a]	...	...	$0.97^{+0.36}_{-0.34}$	$1.17^{+0.07}_{-0.07}$

Notes.—Spectral and timing parameters of the X-ray afterglow evolving phases. The spectra were extracted in the energy range 0.5–6.0 keV with an absorbed power-law fit. The N_H was fixed to the Galactic value of 0.14×10^{22} cm^{-2} due to insufficient statistics at low energies to properly constrain the X-ray absorbing column. We investigated the possibility of internal shocks (the mechanism responsible for the prompt emission) as the origin of the bright second flare, modeling the spectrum with an absorbed cutoff power law and obtaining a better fit to the data than using a simple power law. As can be seen from the photon indices, the choice of the model is critical for determining the hardness of the spectrum. Not enough counts were collected during the first flare to constrain the absorbed cutoff power-law parameters in that time interval, and a simple absorbed power law was used.

[a] Value obtained with C-statistics fit.

structures in the outflow (Nakar et al. 2003), refreshed decelerated shocks by slower shells (Rees & Mészáros 1998), and synchrotron emission from a reverse shock (Kobayashi et al. 2005). The time variability for these models, all related to external shock emission, is longer than the observed time since the GRB trigger (Ioka et al. 2005). Therefore, they are unable to account for the very short timescales of the two flares of GRB 050607, which showed in particular a very steep rise, sharper than for previously reported cases (Romano et al. 2006; Falcone et al. 2006), with values of $\delta t_{rise}/t_{peak} \leq 0.2$, and slower decays with $\delta t_{decay}/t_{peak} \leq 1$. The flares of GRB 050607, unlike the ones previously detected by the XRT, did not have a symmetric shape but were rather similar to the FREDs that are common in the prompt GRB emission and had indication of additional short time variability superimposed on the flares' emission.

The choice of the spectral model to fit the X-ray flares observed is important for a correct interpretation of the data: in the case of GRB 050607, the cutoff power-law model (coincident with a Band function in the XRT energy band) provided a significantly better fit of the brighter flare spectrum than a simple absorbed power law. In addition, the hardness ratio showed that the emission was harder at the flare onset, while the decay was characterized by a softer component. In the late flares detected by *BeppoSAX*, the flare spectral properties were similar to those of the late afterglow, and they were therefore interpreted as the onset of the afterglow itself. The spectral evolution observed during the flares of GRB 050607 suggests instead a mechanism for the origin of the flares distinct from the one responsible for the emission of the underlying decaying afterglow.

The described characteristics observed in the flares of GRB 050607 strongly indicate internal shock emission from late central engine activity at a few hundred seconds after the prompt gamma-ray burst as the origin of the flares. Compared with the three peaks in the prompt emission detected by the BAT, the X-ray flares had lower energies and longer timescales. If the late internal shocks happened at larger radii than those of the prompt gamma-ray emission, smaller magnetic field strength (internal energy density) and a larger curvature timescale (angular spreading timescale) for the shocks would make the resulting flares softer and longer, consistent with our observations. At larger radii the fireball shells should spread and have a larger width, and the observed plateau of the bright flare could be interpreted as produced by a thick shell collision or by a series of collisions.

For a large fraction of *Swift* GRBs, the X-ray afterglow is characterized by a steep to shallow to "normal" behavior (Chincarini et al. 2005; Tagliaferri et al. 2005; Zhang et al. 2006; Nousek et al. 2006; Panaitescu et al. 2006). In the case of GRB 050607,

the flares are presumably superimposed on the steep decay and the transition to the shallow phase is not well constrained. A shallow to normal transition was observed ∼12 ks after the burst. The steepening ($\alpha = 0.58 \pm 0.07$–1.17 ± 0.07) is larger than the value of $\delta\alpha = \frac{1}{4}$ expected when the cooling frequency passes through the observed band in the standard constant energy blast wave model and therefore implies a change of the hydrodynamics of the forward shock, suggesting that the forward shock continues to be refreshed for some time (Zhang et al. 2006; Nousek et al. 2006). In one possible mechanism, the bulk Lorentz factor of the ejecta decreases at the end of the prompt phase, resulting in a monotonic increase of the Lorentz factor with radius. This outflow gradually catches up with the forward shock (blast wave) and gives a smooth energy injection (Sari & Mészáros 2000; Panaitescu et al. 2006). In another scenario, the energy injection originates from a long-lived central engine, active up to a few hours after the prompt emission (Dai & Lu 1998). The decay slope after the break ($\alpha = 1.17$) is consistent with the standard interstellar medium (ISM) forward shock model (Sari et al. 1998). If we apply the standard blast wave model to explain the light curve after 12 ks, an electron index $p \sim 2.2$ is obtained from the decay and spectral indices.

If one assumes that the shallow decay observed in the X-ray energy band originates from refreshed shocks, emission from the associated reverse shocks is expected to peak in the optical band (Sari & Mészáros 2000), with a decay slightly slower than the forward shock emission. The *I*-band decay during the first 6400 s could be modeled with a single power law of index 0.5 (Rhoads 2005b). The measured *I* magnitudes and the X-ray fluxes are consistent within the uncertainties with the model predictions during the shallow phase. With the late measurement of the transient, still detectable in the *I* band 93 ks after the burst trigger (Rhoads 2005c), the *I*-band afterglow decay could be modeled with a single power-law decay with slope 0.4, or 0.3 if the first detection after 640 s was excluded. The fit of the X-ray afterglow decay after the flares with a single power law yields a slope of 0.88. The difference between the reported *I*-band decay and the X-ray slope suggests that the late *I*-band detection had a significant contribution coming from the GRB host galaxy. A new deep observation of the field with ground-based telescopes would verify this interpretation.

APPENDIX

PILE-UP CORRECTION

The pile-up effect causes two or more photons to be considered by the CCD as a single event with energy equal to the sum of the energies of the individual photons. Pile-up, therefore, has a major impact on the observations, by lowering the apparent source count rate and making the apparent spectral index harder (for a detailed discussion, see, for example, Weisskopf et al. [2000]).

Pile-up also modifies the grade distribution of the photons collected on the CCD, via an effect known as "grade migration" (Davis 2001). When an X-ray photon hits the CCD surface, the charge produced is spread over 1 or more pixels; single-pixel events are recorded as "grade 0" events; split-pixel events are designated with higher grades (1–12 for X-ray events; see Burrows et al. [2005b] for the XRT grade definitions). The effect of pile-up is to decrease the number of single-pixel events and to increase the number of apparent multiple-pixel events, depending on the overall incident count rate.

To investigate the extent of the CCD region affected by pile-up, we derived the grade distribution of the events collected from the GRB afterglow during the main flare, when the XRT count rate exceeded 1 count s^{-1}. Annular regions centered on the GRB emission with increasing inner radii and fixed outer radii ($r_{out} = 40$ pixels) were extracted to verify the spatial extent to which the observations are affected by pile-up. The ratio of single-pixel events to the total number of events has been calculated for each annular region, and the results are reported in Table 4. For comparison, ground calibration tests (Moretti et al. 2004) with the XRT showed that in non-piled-up regimes the fraction of single-pixel events is 0.78 at 1.49 keV (the mean photon energy during the bright flare, once the pile-up correction was performed, was measured to be 1.7 keV).

For annular regions with inner radii less than 5 pixels the grade migration effect caused by pile-up is significant, while for inner radii larger than 8 pixels the fraction of single-pixel events remained constant and became comparable with ground calibration measurements for sources with low count rates. To confirm the result, the radial profile of the bright flare was extracted and compared with the analytical PSF described in Moretti et al. (2004). The two profiles showed little or no deviations at radii larger than 8 pixels. To avoid the region affected by pile-up while minimizing the number of rejected events in the central region, the analysis of the GRB afterglow during the bright flare was performed using an annular region that excluded events in the central 8 pixels (18″88) and with an outer radius of 40 pixels.

The number of events rejected from the central 8 pixels is in principle dependent on the incident spectrum and the details of the energy-dependent PSF. For a point source at 2′ from the center of the CCD (as is the case of the GRB 050607 X-ray afterglow during the first orbit), 80% of the PSF is included in an 8 pixel circle at an energy of 0.5 keV, 77% at 1.7 keV (the mean energy of the flare spectrum corrected for pile-up), and 74% at 3.0 keV. We therefore used XSPEC version 11.3.2 to calculate the correction factor for the pile-up. The spectra from the annular region and the background region were extracted; the xrtmkarf command (ver. 0.4.14) was used to create two ancillary response files, with and without applying the PSF correction. Fitting the spectrum with an absorbed power-law model we obtained the best-fit parameters for the two ancillary response files. The ratio of the two normalization parameters yields the correction factor to account for the effect of pile-up. The coefficient ($c_{pile-up} = 0.20 \pm 0.03$) obtained from the spectral analysis was used to multiply the count rate observed in the annular region and is consistent with the fraction of PSF contained in the 8 pixel central region.

TABLE 4
GRB 050607: Grade Distribution

Inner Radius (pixels)	Events	Single-Pixel Events	Fraction of Total Events (%)
0	1774	1131	63.7
5	1092	805	73.7
6	958	726	75.8
7	806	631	78.3
8	718	569	79.2
9	634	511	80.6
10	567	456	80.4
15	362	292	80.6

REFERENCES

Band, D., et al. 1993, ApJ, 413, 281
Barthelmy, S., et al. 2005, Space Sci. Rev., 120, 143
Burrows, D. N., et al. 2005a, Science, 309, 1833
———. 2005b, Space Sci. Rev., 120, 165
Cash, W. 1979, ApJ, 228, 939
Chincarini, G., et al. 2005, ApJ, submitted (astro-ph/0506453)
Dai, Z. G., & Lu, T. 1998, A&A, 333, L87
Davis, J. E. 2001, ApJ, 562, 575
Dickey, J. M., & Lockman, F. J. 1990, ARA&A, 28, 215

Falcone, A. D., et al. 2006, ApJ, 641, 1010
Galli, A., & Piro, L. 2005, A&A, submitted (astro-ph/0510852)
Gehrels, N., et al. 2004, ApJ, 611, 1005
Godet, O., et al. 2006, A&A, in press
Halpern, J. P., Kemp, J., & Mirabal, N. 2005a, GCN Circ. 3530, http://gcn.gsfc.nasa.gov/gcn/gcn3/3530.gcn3
———. 2005b, GCN Circ. 3541, http://gcn.gsfc.nasa.gov/gcn/gcn3/3541.gcn3
Hill, J. E., et al. 2004, Proc. SPIE, 5165, 217
Ioka, K., Kobayashi, S., & Zhang, B. 2005, ApJ, 631, 429

Ivanushkina, M., Retter, A., McGowan, K., Blustin, A., & Gehrels, N. 2005, GCN Circ. 3537, http://gcn.gsfc.nasa.gov/gcn/gcn3/3537.gcn3

Kobayashi, S., Zhang, B., Mészáros, P., & Burrows, D. N. 2005, ApJ, submitted (astro-ph/0506157)

Lazzati, D., Rossi, E., Covino, S., Ghisellini, G., & Malesani, D. 2002, A&A, 396, L5

Mészáros, P., & Rees, M. J. 1997, ApJ, 476, 232

Moretti, A., et al. 2004, Proc. SPIE, 5165, 232

———. 2006, A&A, 448, L9

Nakar, E., Piran, T., & Granot, J. 2003, NewA, 8, 495

Nousek, J. A., et al. 2006, ApJ, 642, 389

Paciesas, W. S., et al. 1999, ApJS, 122, 465

Panaitescu, A., Mészáros, P., Gehrels, N., Burrows, D. N., & Nousek, J. A. 2006, MNRAS, 366, 1357

Piro, L., et al. 2005, ApJ, 623, 314

Preece, R. D., et al. 2000, ApJS, 126, 19

Rees, M. J., & Mészáros, P. 1998, ApJ, 496, L1

Retter, A., et al. 2005, GCN Circ. 3525, http://gcn.gsfc.nasa.gov/gcn/gcn3/3525.gcn3

Rhoads, J. 2005a, GCN Circ. 3527, http://gcn.gsfc.nasa.gov/gcn/gcn3/3527.gcn3

———. 2005b, GCN Circ. 3531, http://gcn.gsfc.nasa.gov/gcn/gcn3/3531.gcn3

———. 2005c, GCN Circ. 3540, http://gcn.gsfc.nasa.gov/gcn/gcn3/3540.gcn3

Romano, P., et al. 2006, A&A, 450, 59

Roming, P., et al. 2005, Space Sci. Rev., 120, 95

Sari, R., & Mészáros, P. 2000, ApJ, 535, L33

Sari, R., Piran, T., & Narayan, R. 1998, ApJ, 497, L17

Tagliaferri, G., et al. 2005, Nature, 436, 985

Testa, V., et al. 2005, GCN Circ. 3538, http://gcn.gsfc.nasa.gov/gcn/gcn3/3538.gcn3

Weisskopf, M. C., et al. 2000, ApJ, 536, L81

Zhang, B., Fan, Y. Z., Dyks, J., Kobayashi, S., Mészáros, P., Burrows, D. N., Nousek, J. A., & Gehrels, N. 2006, ApJ, 642, 354